Journal Name

ARTICLE TYPE

Cite this: DOI: 00.0000/xxxxxxxxxx

Mutual information does not detect growing correlations in the propensity of a model molecular liquid†

Antonio Tripodo,[a] Andrea Giuntoli,[a] Marco Malvaldi,[a] and Dino Leporini[ab]*

Received Date
Accepted Date

DOI: 00.0000/xxxxxxxxxx

The dynamical spatial correlations detected by the mutual information (MI) in the isoconfigurational particle displacements of a monodisperse molecular viscous liquid are studied via molecular-dynamics simulations by changing considerably both the molecular mobility and the degree of dynamical heterogeneity. Differently from atomic liquids, the MI correlation length is not growing on approaching the glass transition by considering the liquid both in full detail as a collection of monomers and as a coarse-grained ensemble of molecular centers of mass. In the detailed picture it is found that: i) the MI correlations between monomers are largely due to inter-molecular correlations, ii) the MI length scale is numerically identical, within the errors, to the correlation length scale of the displacement direction, as drawn by conventional correlation functions. The time evolution of the MI spatial correlations complies with the scaling between the fast vibrational dynamics and the long-time relaxation. Our findings suggest that the characteristics of the MI length scale are markedly system-dependent and not obviously related to dynamical heterogeneity.

1 Introduction

The nature of the solidification process observed at the glass transition temperature T_g by cooling supercooled viscous liquids is a topic of intense research[1,2]. Starting with the seminal paper by Adam and Gibbs, who invoked the presence of "cooperatively rearranging regions" in viscous liquids[3], increasing interest has been devoted to identifying possible growing length scales as mobility decreases (for a recent topical review see ref.[4]). A broad classification in terms of either static or dynamic length scales is usually used. Static (thermodynamic) length scales are determined by the free energy landscape, whereas dynamic length scales are set by the rules governing the time evolution of the system and extracted from finite-time behavior of time-dependent correlation functions and associated susceptibilities. Even if growing static length scales have been reported by experiments[5] and simulations[6], there is still debate if they control the glass transition[7]. On the other hand, the discovery of the spatial inhomogeneity of the dynamics in supercooled liquids, the so-called dynamic heterogeneity, e.g. see the review[8], revealed that more and more particles move in a correlated way approaching T_g from above and promoted the study of their characteristic dynamical length scales[9]. It is still not clear to what extent dynamic correlations are the consequence or the primary origin of slow dynamics[4].

The present paper investigates dynamic spatial correlations detected by mutual information (MI). MI is a measure of the degree of statistical dependence (correlation) of two random variables X and Y[10,11]. Notably, MI, differently from the usual correlation coefficient, can capture the nonlinear dependence between two random variables[12]. MI is defined as[10,11]:

$$I(X,Y) = \int\int dx\,dy\; p(x,y) \log\left[\frac{p(x,y)}{p(x)p(y)}\right] \qquad (1)$$

where $p(x,y)$ is the joint probability distribution of the random variables X and Y with distributions $p(x)$ and $p(y)$, respectively. MI has been used for detecting classical phase transitions for several classical system and topological transition in the XY model[13], the phase transition in a 2D disordered Ising model[14] and for evaluating the configurational entropy of liquid metals[15]. In the framework of liquid-state physics MI has been considered in *atomic* glassformers as a metric of the correlation between structural and dynamical quantities[16–18], in particular the propensity[17,18]. We remind that propensity refers to particle displacements starting from the same initial global configuration and is a tool to investigate the possible link between structure and dynamics[19].

As a follow-up of previous studies[20,21], we adopt the scheme of ref.[18] and investigate by molecular-dynamics (MD) numerical simulations the MI correlations in space and time of the propen-

[a] *Dipartimento di Fisica "Enrico Fermi", Università di Pisa, Largo B.Pontecorvo 3, I-56127 Pisa, Italy*
[b] *Istituto per i Processi Chimico-Fisici-Consiglio Nazionale delle Ricerche (IPCF-CNR), via G. Moruzzi 1, I-56124 Pisa, Italy*
* *Fax: +390502214333; Tel: +390502214937; E-mail: dino.leporini@unipi.it*

sities of a model *molecular* glassformer. As a major result, we find *no growing dynamical correlations* on slowing down the microscopic mobility. This finding is strikingly different with respect to the outcomes of MI studies of atomic glassformers where a clear *increase* has been reported [18].

2 Models and methods

We performed molecular-dynamics (MD) simulations of fully-flexible, i.e. with no bond-bond bending potential, linear chains of trimers ($M = 3$) in the supercooled regime. All simulations were carried out with the open-source software LAMMPS [22,23]. Non-bonded monomers interact with a truncated Lennard-Jones potential

$$U^{LJ}(r) = \varepsilon \left[\left(\frac{\sigma^*}{r} \right)^{12} - 2 \left(\frac{\sigma^*}{r} \right) \right] + U_{cut}(r) \tag{2}$$

where $\sigma^* = 2^{1/6}\sigma$ is the location of the potential minimum which has depth ε. U_{cut} is chosen to ensure $U^{LJ}(r) = 0$ for any $r > r_{cut}$ and r_{cut} is set to the value of 2.5σ. Monomers that belongs to the same chain interact with each other via the harmonic potential

$$U^b(r) = k(r - r_0)^2 \tag{3}$$

where the constant k is set to $555.5\varepsilon/\sigma^2$ and the rest length of the bond is $r_0 = 0.97\sigma$. All quantities are in reduced units: length in units of σ, temperature in units of ε/k_B and time in units of $\sigma\sqrt{m/\varepsilon}$ where m is the monomer mass [24]. We set $m = k_B = 1$. The time step for the integration was chosen to be 0.003. All the investigated systems have $N = 3999$ monomers, i.e. 1333 chains. The NVT ensemble has been used for the equilibration runs. For each run the equilibration time lasted not less than $3\tau_{ee}$, where τ_{ee} is the end to end vector autocorrelation function decay time [25–28]. After equilibration, the NVE ensemble was employed for the data production employing at least sixteen independent runs. We built three sets of states varying both the density ρ and temperature T, each state being characterized by the pair (ρ, T): set A [(1.05, 0.60), (1.01, 0.47)], set B [(1.01, 0.435), (1.03, 0.49)], set C [(1.05, 0.51), (1.02, 0.42)]. The states of the same set exhibit the same relaxation time τ_α, i.e. $\tau_\alpha^{(A)} \simeq 42$, $\tau_\alpha^{(B)} \simeq 150$, $\tau_\alpha^{(C)} \simeq 1550$. The exact definition of the relaxation time will be given in Sec.3.1.

From the equilibrated configuration of each state, in parallel to the usual production runs in NVE ensemble, we also started production runs in the iso-configurational ensemble (ICE) [19]. Each ICE, henceforth labeled by μ, consists of a single initial spatial configuration of all the particles, each of them starting the time evolution with 1000 random assignments of the initial velocity, as drawn from the corresponding Maxwell-Boltzmann distribution of the state. We considered four ICEs for the states of the set C and two ICEs for the other two sets, in close agreement with other studies performed with about three times less particles than the present one [18]. The initial configurations of the ICEs were randomly taken by the set of NVE production runs. The fact that the number of ICEs is less than the number of production runs in the NVE ensemble is due to the extremely time-consuming procedure to perform the MI evaluation. Arguments will be presented in Sec.3 to conclude that the phase space explored by all the ICEs of a single state is indistinguishable from the one explored by all the NVE runs.

To perform the MI evaluation, if the distribution functions which are involved in the MI definition, Eq.1, are unknown, one has to resort to complex estimators. Following previous studies [17,18], we employed the Kraskov-Stögbauer-Grassberger estimator [11]. The high number of velocity assignments in each ICE ensures proper convergence of the estimator.

3 Results and discussion

3.1 Relaxation and transport

We first characterize the relaxation and the mobility of the molecular liquid. One central quantity is the self part of the van Hove function $G_s(\mathbf{r},t)$ [29]:

$$G_s(\mathbf{r},t) = \frac{1}{N} \left\langle \sum_{i=1}^{N} \delta\left[\mathbf{r} + \mathbf{r}_i(0) - \mathbf{r}_i(t)\right] \right\rangle \tag{4}$$

where $\mathbf{r}_i(t)$ is the position of the i-th monomer at time t and the brackets denote the average over the system replicas. In isotropic liquids the van Hove function depends on the modulus r of $\mathbf{r}$. The interpretation of $G_s(r,t)$ is direct. The product $G_s(r,t) \cdot 4\pi r^2$ is the probability that the monomer is at a distance between r and $r+dr$ from the initial position after a time t. The second moment of the van Hove function is the mean square displacement (MSD):

$$\langle \delta r^2(t) \rangle = \frac{1}{N} \sum_{j=1}^{N} \left\langle ||\mathbf{r}_j(t) - \mathbf{r}_j(0)||^2 \right\rangle \tag{5}$$

The spatial Fourier transform of the self part of the van Hove function yields the self part of the intermediate scattering function (ISF) [29]:

$$F_s(\mathbf{q},t) = \frac{1}{N} \left\langle \sum_{j=1}^{N} e^{i\mathbf{q}\cdot[\mathbf{r}_j(t) - \mathbf{r}_j(0)]} \right\rangle \tag{6}$$

which in an isotropic liquid depends only on the modulus of the wavevector $q = ||\boldsymbol{q}||$. ISF provides a convenient relaxation function to study the rearrangements of the spatial structure of the fluid over the length scale $\sim 2\pi/q$. We define the structural relaxation time τ_α by the relation $F_s(q_{max}, \tau_\alpha) = e^{-1}$ where q_{max} is the maximum of the static structure factor (for the present study $7.14 \leq q_{max} \leq 7.22$).

The top panel of Fig.1 shows the monomer ISF of all the states under investigation. To better understand the relaxation process, the top inset also plots the monomer MSD. The coincidence of the ISF and MSD curves of particular states over all the time window will be commented at the end of the present Sec. 3.1. At very short times (ballistic regime) MSD increases according to $\langle r^2(t) \rangle \cong (3k_BT/m)t^2$ and ISF starts to decay. At later times, the repeated collisions with the other monomers slow the displacement of the tagged one and a quasi-plateau region, also found in ISF, occurs when the temperature is lowered and/or the density increased. This signals the increased caging of the particle. The latter is released by the cage after an average time τ_α, leading to the ISF decay and the MSD increase due to diffusive motion for $t \gtrsim \tau_\alpha$. It is worth noting that no difference is observed if ISF and MSD

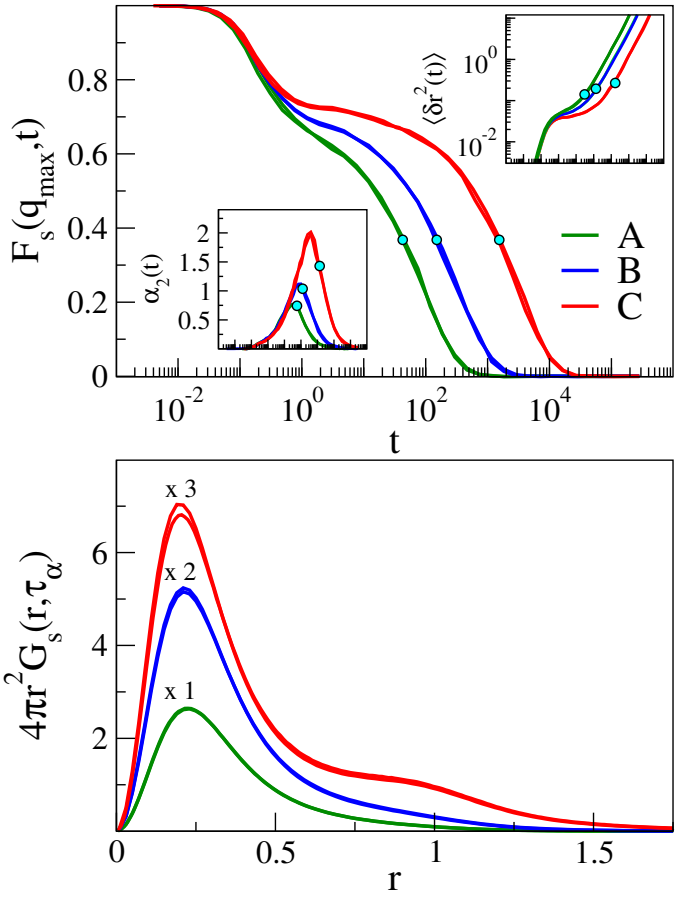

Fig. 1 Top: ISF, Eq.6, at q_{max}, the first peak of the static structure factor, of the six studied states. ISFs are groupable in three distinct pairs. The relaxation time τ_α of each pair is marked by a dot. Insets: MSD, Eq.5, and NGP, Eq.7. Bottom: self-part of the van Hove function $G_s(r,\tau_\alpha)$, Eq.4. The states of the C set reveal a bimodal structure of the van Hove function signalling marked heterogeneous dynamics in agreement with their highest NGP maximum. Note that, if two ISF, MSD and NGP curves coincide at short time ($t \sim 1$), they do the same up to τ_α at least. This is a manifestation of the known universal scaling between the fast vibrational dynamics and the long-time relaxation in viscous liquids[30,31]. See text for details.

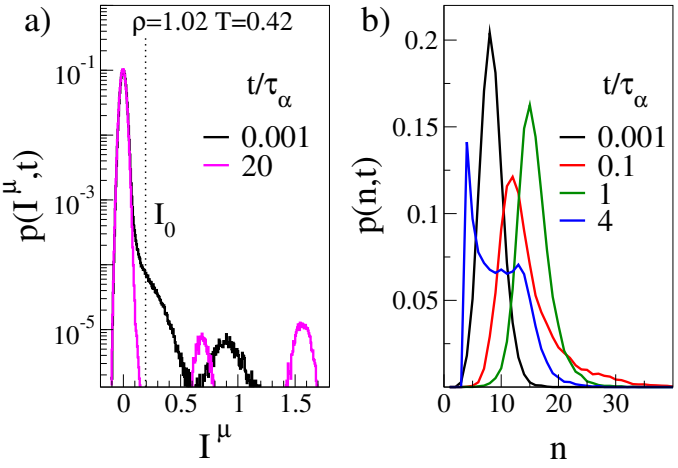

Fig. 2 Panel (a): representative plots of the MI distribution at time t for a single ICE of a selected state of the C set. The threshold $I_0 = 0.2$ above which MI values are considered significant[18] is also indicated. Panel (b): distribution $p(n,t)$ of the number of correlated particles with a central one at time t. The distribution is averaged over all ICEs of the state of the panel (a).

are evaluated in terms of the ICEs instead of the NVE runs (not shown). The bottom inset of the top panel of Fig.1 shows the non-gaussian parameter (NGP) to be defined as:

$$\alpha_2(t) = \frac{3 < \delta r^4(t) >}{5 < \delta r^2(t) >^2} - 1 \qquad (7)$$

$\alpha_2(t)$ vanishes if the displacement r is gaussian and is a well-known metric of the dynamical heterogeneity, featuring the non-gaussian character of the displacements[1,2,8]. It is seen that the maximum of $\alpha_2(t)$ increases with the relaxation time and states with equal relaxation time have virtually identical $\alpha_2(t)$[30,32]. The increasing peak height of $\alpha_2(t)$ proves that the states have significantly different dynamical heterogeneity. Fig. 1(bottom) presents the self-part of the van Hove function $G_s(r,t)$ evaluated at τ_α of the three sets of states. It is seen that states with equal τ_α (the sets A, B, C) have coinciding $G_s(r,\tau_\alpha)$ in agreement with previous studies[31,33]. Most monomers displace by half a radius, $r \sim 0.25$. The states of the set C also exhibit a secondary peak at $r \sim 1$ (the monomer diameter) due to the presence of fast particles with jump dynamics[34], revealing strong heterogeneous dynamics in agreement with the higher NGP peak than the A and B sets.

It is worth noting that the six states of the present study are designed to emphasise the noted universal scaling between the fast vibrational dynamics and the long-time relaxation in viscous liquids[20,21,30,31,33,35–48]. The scaling states that, considering any ensemble-averaged time-dependent quantity $X(t)$, if two physical states exhibit equal value of $X(t)$ at very short times ($t \sim 1$, corresponding to a few picoseconds[49]), the time evolution of $X(t)$ in the two states is the same up to τ_α at least. Fig.1 illustrates the scaling for ISF, MSD and NGP by showing that their curves referring to *six different states are groupable over the whole time window in three separate pairs, each labelled by a specific τ_α value*. The scaling also holds for the van Hove function[31,33] and explains the grouping of the van Hove functions in Fig.1(bottom). On this basis, a further goal of the present study is to test the scaling in the framework of MI correlations in the isoconfigurational ensemble.

3.2 Mutual Information

3.2.1 Global distribution

Fig.2(a) presents representative plots of the distribution $p(I^\mu,t)$ of the MI values at time t for a single ICE of the liquid, i.e. $p(I^\mu,t)dI^\mu$ is the probability that the MI between two particles at time t is located in the range $[I^\mu, I^\mu + dI^\mu]$. The MI of the particle pair (i,j) is evaluated, according to Eq.1, by the relation

$$I^\mu_{ij}(t) = I(\delta\vec{r}^\mu_i(t), \delta\vec{r}^\mu_j(t)) \qquad (8)$$

where $\delta\vec{r}^\mu_i(t)$ is the displacement of the i-th particle in a time t starting from the initial position in the selected ICE. The particles i and j are said to be correlated at time t if $I^\mu_{ij}(t) > I_0$ with $I_0 = 0.2$.

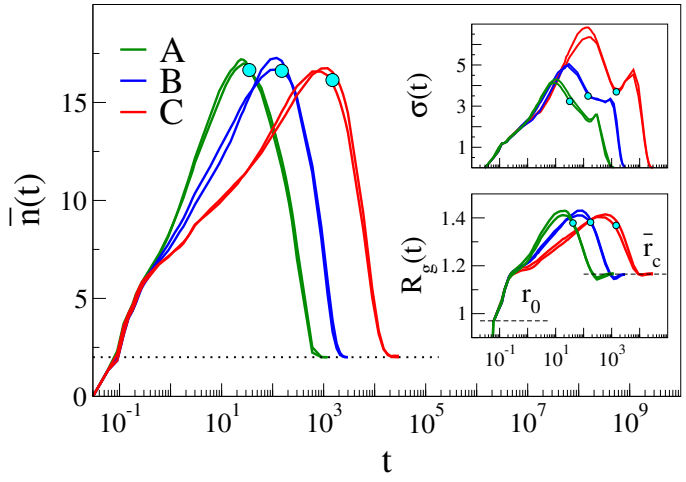

Fig. 3 Time-dependence of the average number of particles correlated with a central one $\bar{n}(t)$. Color codes as in Fig.1. Insets: time-dependence of the standard deviation $\sigma(t)$ (top) and the gyration radius of the clusters of correlated particles $R_g(t)$ [18] (bottom). r_0 and $\bar{r}_c$ denote the bond length and the average distance between the monomers belonging to the same molecule, respectively. States with equal relaxation time, marked by dots, exhibit coincident time dependence of $\bar{n}(t)$, $\sigma(t)$ and $R_g(t)$, thus supporting the universal scaling between the fast vibrational dynamics and the long-time relaxation in viscous liquids [20,21,30,31,33,35–48].

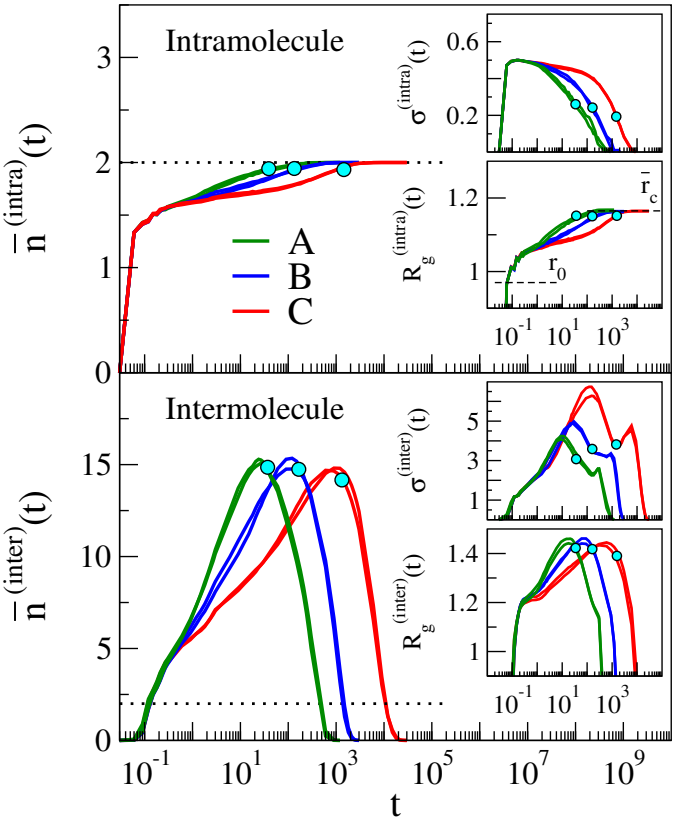

Fig. 4 Time-dependence of the average number of particles correlated with a central one $\bar{n}(t)$ belonging to the same molecule (top panel) or different molecules (bottom panel). Color codes as in Fig.1. The insets of both panels refer to the time-dependence of the standard deviation $\sigma(t)$ and the gyration radius of the clusters of correlated particles $R_g(t)$ [18]. r_0 and $\bar{r}_c$ as in Fig.3 . States with equal relaxation time, marked by dots, exhibit coincident time dependence of $\bar{n}^{(x)}(t)$, $\sigma^{(x)}(t)$ and $R_g^{(x)}(t)$ with x $\in$ {inter, intra} over all the time window, supporting the universal scaling between the fast vibrational dynamics and the long-time relaxation.

The threshold value I_0 has been chosen in agreement with other studies [18] to filter out the contributions at small MI values where the MI estimator is less reliable [11] . Fig.2 (a) shows that for $t \ll \tau_\alpha$ the distribution $p(I^\mu,t)$ exhibits a bimodal structure above I_0 which develops as two well separated peaks at $t \gg \tau_\alpha$. The two peaks stem from the permanent bonds linking a monomer to the other two ones of the trimer, establishing permanent MI. Preliminary runs show that nine peaks are seen in decamers at long times. The multi-modal structure of $p(I^\mu,t)$ is missing in atomic liquids [18]. Fig.2(b) plots, for the same state considered in Fig.2(a), the distribution of the number of particles correlated to a central one at time t, $p(n,t)$. The distribution is averaged over all the ICEs of the state. In the ballistic regime $p(n,t)$ peaks at very small n values, but the maximum steeply increases with time for $t \lesssim \tau_\alpha$ due to rapid exploration of the cage by the central particle, establishing correlations with the neighbours. For $t \sim 0.1\tau_\alpha$, the distribution $p(n,t)$ broadens and becomes skewed. At $t \sim \tau_\alpha$ the distribution narrows. Finally, at $t \sim 4\tau_\alpha$, the distribution broadens asymmetrically again with a notable change of the shape indicating two distinct families of correlated particles. A similar behaviour has been reported in *atomic* liquids [18].

Fig.3 plots two characteristic parameters of of the distribution $p(n,t)$, i.e. the average number of correlated particles with a central one $\bar{n}(t)$ (main panel) and the standard deviation $\sigma(t)$ (top inset). It also plots the gyration radius $R_g(t)$, the average distance between correlated particles [18] (bottom inset). Notably, states with *equal* relaxation time exhibit, within the errors, the *same* time dependence of $\bar{n}(t)$, $\sigma(t)$ and $R_g(t)$ in the whole range, covering both vibrational and relaxation time scales. We interpret the finding as a manifestation of the aforementioned scaling between the fast vibrational and the slow dynamics in glassforming systems [20,21,30,31,33,35–48]. Fig.3 shows that the average $\bar{n}(t)$ vanishes at short times, peaks at $t \sim \tau_\alpha$ and eventually reaches at long time the plateau level corresponding to the fact that in a molecule each particle has permanent correlations with two other monomers. The gyration radius starts at very short times at $R_g \sim r_0$, i.e. the bond length, and levels off at long times at the plateau $\bar{r}_c$, corresponding to the average distance between the monomers of a molecule, as evaluated by, e.g., the intrachain radial distribution function [50]. The complex pattern of the standard deviation is rather close to the one of atomic liquids [18] and will be discussed in a forthcoming paper.

Fig.3 shows a central result of the paper. It is seen that, changing the relaxation time by a factor of ~ 40 does *not* change the maxima of two metrics of the spatial correlations, i.e. the average number of correlated particles with a central one $\bar{n}(t)$ and the gyration radius R_g. *This is in striking contrast with the behaviour of atomic liquids where the maxima of both $\bar{n}(t)$ and R_g are seen to increase with the structural relaxation time* [18]. We have checked that changing I_0 in the range $0.1 \leq I_0 \leq 0.3$ does not affect this finding.

3.2.2 Intermolecular and intramolecular distribution

Fig.4 provides further insight into the time evolution of the distribution of the correlated particles to a central one belonging to the *same* molecule (top) or *other* molecules (bottom). As in Fig.3, we focus on the average, the standard deviation and the gyration radius, i.e. the average distance between correlated particles. They are referred to as $\bar{n}^{(x)}(t)$, $\sigma^{(x)}(t)$ and $R_g^{(x)}(t)$ for intramolecular ($x = intra$) and intermolecular ($x = inter$) correlations, respectively. Fig.4(top) shows that the average number of correlated particles belonging to the *same* molecule grows with *two* distinct regimes. A *fast* increase, developing within $t \sim 1$, corresponding to the full exploration of the surrounding cage by the monomer[30], and a much *slower* growth to reach the asymptotic level, 2, which completes within the structural relaxation time τ_α. The standard deviation exhibits a fast increase followed by a slow decay denoting the stable character of the intramolecular correlation due to monomer mutual bonding, whereas the gyration radius increases qualitatively above the bond length value, r_0, to reach the same asymptotic value of the global gyration radius, see Fig.3. Fig.4(bottom) refers to the correlation between a monomer and other ones belonging to *different* molecules. It is seen that the time evolution of the average number of correlated particles belonging to *different* molecules, $\bar{n}^{(inter)}(t)$, behaves qualitatively like the global average $\bar{n}(t)$ for $t \lesssim \tau_\alpha$. In particular, the maximum value of $\bar{n}^{(inter)}(t)$, reached close to $t \sim \tau_\alpha$, does *not* increase by increasing the structural relaxation times and one has $\bar{n}^{(inter)}(\tau_\alpha) \simeq \bar{n}(\tau_\alpha) - 2$. This approximate relation points out that most particles correlating to a monomer belong to a *different* molecule. Consistent with the latter finding, a near coincidence between the global and the intermolecular gyration radiuses is also observed $R_g^{(inter)}(t) \simeq R_g(t)$ for $t \lesssim \tau_\alpha$, including their maximum value. At long times, differently from $R_g(t)$, $R_g^{(inter)}(t)$ vanishes since the central particle has no permanent correlations with the ones of other molecules. Finally, we notice that the standard deviation of the global distribution of correlated particles, $\sigma(t)$ is set by the *intermolecular* contribution. In fact, $\sigma^{(inter)}(t) \simeq \sigma(t)$, see the top inset of Fig.4(bottom).

3.2.3 Molecular center-of-mass distribution

Instead of considering the molecular liquid as a collection of N monomers, we may picture it in a coarse-grained way as a collection of $N/3$ point particles, each localised at the molecular center of mass. The MI distribution between the molecular centers of mass is of interest to investigate the MI correlations at the molecular level going beyond the local fast modes internal to the molecule itself. It is also useful as a tool to compare the MI correlations of our monodisperse molecular liquid with the reported ones of a polydisperse atomic liquid[16–18] in that maps the former to an effective atomic one. Fig.5 plots the average number $\bar{n}^{(cm)}(t)$ and the standard deviation $\sigma^{(cm)}(t)$ of the MI distribution between the molecular centers of mass. We see that the maximum of $\bar{n}^{(cm)}(t)$, as the maximum of $\bar{n}(t)$ (see Fig.3), does not increase by increasing the relaxation time. Notably, the maximum occurs at a time earlier than τ_α close to - but not coincident with - the time where the maximum of the non-gaussian parameter $\alpha_2(t)$ is located, see inset of Fig.1 (top). A qualitative resemblance of

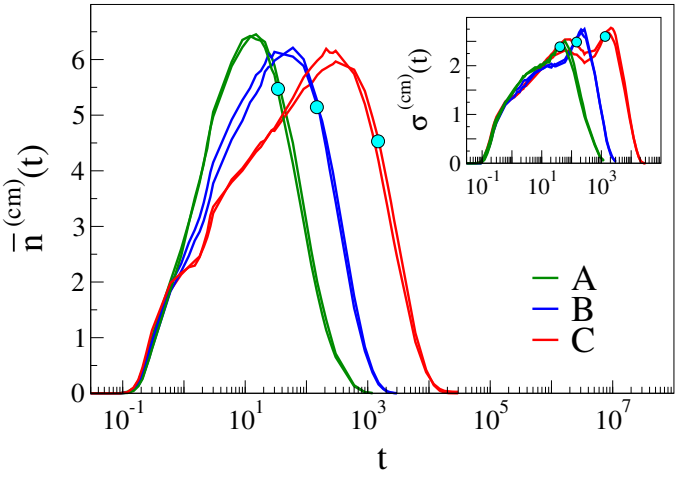

Fig. 5 Time-dependence of the average number of center-of-mass correlated with a central one according to MI ($\bar{n}^{(cm)}(t)$). Inset: standard deviation ($\sigma^{(cm)}(t)$). Color codes as in Fig.1. States with equal relaxation time, marked by dots, exhibit coincident time dependence of $\bar{n}^{(cm)}(t)$ and $\sigma^{(cm)}(t)$ over all the time window, supporting the universal scaling between the fast vibrational dynamics and the long-time relaxation.

$\sigma^{(cm)}(t)$ with the global standard deviation $\sigma(t)$ (Fig.3, top inset) is noted.

3.2.4 Dynamical correlation lengths

To better scrutinize the MI spatial correlations, we consider the average MI value, $\bar{I}(r,t)$ which is defined as the average of $I_{ij}^{\mu}(t)$ defined in Eq.8, over all the i and j particles spaced by r in the initial configuration of a given ICE and further averaged over all the ICEs. We focus on $t = \tau_\alpha$. Fig.6 plots the average MI spatial correlations at τ_α, $\bar{I}(r,\tau_\alpha)$ for all the states under investigation. Apart from a mild modulation, in-phase with the radial distribution function, only a weak dependence on the state is seen, consistently with Fig.3. The slope ξ_I of the exponential tail in a log-lin plot provides a measure of the MI correlation length[18]. We point out that the above definition of the correlation length, involving an average over all the monomers, parallels the average performed over all the particles of the five-component atomic mixture carried out in ref.[18]. Picturing our system not as a collection of monomers but as a coarse-grained collection of molecular centers of mass and repeating the above procedure yields the alternative dynamical correlation length $\xi_{I_{CM}}$. The inset of Fig.6 shows that, in agreement with the findings of Fig.3 and Fig.6, *both ξ_I and $\xi_{I_{CM}}$ increase very weakly on approaching the glass transition* (the former by about 8.5% and the latter by about 2.5%, to be compared with $\sim 30\%$ in atomic liquids in nearly the same range of relaxation time values[18]). Notice that evaluating $\xi_{I_{CM}}$ not at τ_α but at the time when $\bar{n}^{(cm)}(t)$ is maximum upshifts the correlation length to $\xi'_{I_{CM}}$. The latter differs from $\xi_{I_{CM}}$ by less than 3% and increases like $\xi_{I_{CM}}$ by increasing the structural relaxation time.

Alternative dynamical correlation lengths may be drawn by considering spatial displacement-displacement correlations (DDC) via suitable correlation functions averaged in the NVE ensemble[20,21]. To this aim, we define two distinct correlation func-

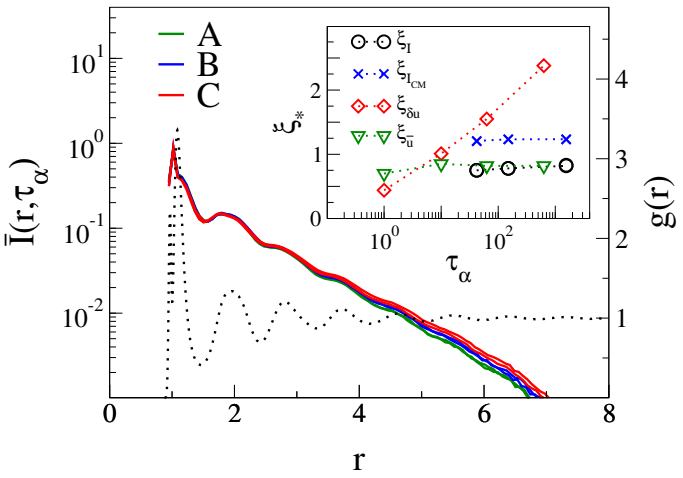

Fig. 6 Average mutual information at τ_α between the central monomer and a surrounding one at r distance for all the states under investigation. The slope of the exponential tail defines the MI correlation length ξ_I. The same procedure applied to the molecular center of mass yields the correlation length $\xi_{I_{CM}}$ (see text for details). Color codes as in Fig.1. The dotted line is the radial distribution function (negligibly state-dependent). The sharp peak at $r \sim r_0 \sim 0.97$ is due to bonded particles. Inset: MI correlation lengths ξ_I and $\xi_{I_{CM}}$ superimposed to the ones of the modulus ($\xi_{\delta u}$) and the direction ($\xi_{\vec{u}}$) of the particle displacement in the NVE ensemble[20,21]. Error bars are smaller than the symbol size.

tions considering DDC restricted to the direction (D-DDC) and the modulus, i.e. mobility, (M-DDC)[20,21]. More explicitely, the D-DDC, $C_{\vec{u}}(r,t)$ and M-DDC, $C_{\delta u}(r,t)$ correlation functions are defined as

$$C_{\vec{u}}(r,t) = \langle \hat{\mathbf{u}}_i(t_0,t)\cdot\hat{\mathbf{u}}_j(t_0,t)\rangle, \quad (9)$$

$$C_{\delta u}(r,t) = \frac{\langle \delta u_i(t_0,t)\delta u_j(t_0,t)\rangle}{\langle[\delta u(t_0,t)]^2\rangle}. \quad (10)$$

$\hat{\mathbf{u}}_k(t_0,t)$ is the versor of the displacement of k-th monomer in a time interval from t_0 to t_0+t:

$$\mathbf{u}_k(t_0,t) = \mathbf{r}_k(t_0+t) - \mathbf{r}_k(t_0) \quad (11)$$

whereas the deviation from the average of the modulus of the displacement of k-th monomer in the same time interval is defined as:

$$\delta u_k(t_0,t) = |\mathbf{u}_k(t_0,t)| - \langle|\mathbf{u}(t_0,t)|\rangle \quad (12)$$

An average over all the i-th and j-th monomers spaced by r at time t_0 is understood in Eq.9 and Eq.10. On increasing r, both $C_{\vec{u}}(r,\tau_\alpha)$ and $C_{\delta u}(r,\tau_\alpha)$ exhibit an exponential tail with slopes $\xi_{\vec{u}}$ and $\xi_{\delta u}$ in a log-lin plot, respectively[20,21]. It has been reported that $\xi_{\vec{u}}$ and $\xi_{\delta u}$ behave in a different way by increasing the structural relaxation time τ_α, i.e. the former is virtually constant whereas the latter shows a marked increase[20,21]. This distinction is *not* related to the molecular character of the liquid in that it has been also reported in a binary *atomic* mixture[51]. The different character of $\xi_{\vec{u}}$ and $\xi_{\delta u}$ may be rationalised. First, let us consider $\xi_{\vec{u}}$. In the present model molecular liquid the D-DDCs between a central particle and the closer ones, following their mutual collisions, are apparent only in the nearest shells where set in very fast (within $t \sim 1$, corresponding to a few picoseconds[49]) [52]. The above findings suggest that D-DDCs are very local, as also confimed by the fact that $\xi_{\vec{u}}$ is of the order of the monomer size, and then less related to the large-scale cooperative rearrangements setting the structural relaxation. Now, let us consider $\xi_{\delta u}$. The latter provides a measure of the size of the regions where the *local* mobility differs from the average *global* mobility. In the phenomenon of dynamical heterogeneity the liquid may be thought as partitioned in clusters of particles with different mobility[8,9,20]. Then, one expects that, on cooling from high temperature where the liquid is dynamically homogeneous, $\xi_{\delta u}$ increases on approaching the glass transition. Even if related to the dynamic heterogeneity, the detailed microscopic mechanism leading to the increase of $\xi_{\delta u}$ needs further investigation. Given the known link between relaxation and elasticity in molecular liquids and polymers[53,54], an interesting approach is provided by the rigidity percolation scenario[55].

The inset of Fig.6 shows that $\xi_I \sim \xi_{\vec{u}}$, i.e. the MI length is nearly constant and rather close to the one of the D-DDC, whereas it is rather decoupled from the correlation length of the mobility which senses more effectively the dynamical heterogeneity. The finding that MI correlation decouple from M-DDC will be investigated in future studies. Preliminarily, we note that Eq.1 is invariant under affine changes. As a consistency test, we have found that Eq.8 is invariant under the global scale change $\delta\vec{r}_k^{\,\mu}(t) \to \lambda\,\delta\vec{r}_k^{\,\mu}(t)$.

4 Conclusions

We studied by MD simulations the transport and the relaxation of a model *molecular* liquid in the NVE and the isoconfigurational ensembles by changing considerably *both the molecular mobility and the degree of dynamical heterogeneity*. We focus on the MI correlation length which is observed to increase in atomic liquids on approaching the glass transition. We find that the time evolution of the MI spatial correlations complies with the scaling between the fast vibrational dynamics and the long-time relaxation. We evidence that the MI correlations between monomers are largely due to inter-molecular correlations. We also find that, considering the liquid as a collection of monomers, the MI correlation length is *weakly dependent on the structural relaxation time*, virtually coincident with the length scale of the direction correlation of the particle displacement and decoupled from mobility spatial correlations sensing the dynamical heterogeneity. Similarly, adopting the coarse-grained picture of the molecular liquid as a collection of point particles localised at the molecular centers of mass leads to an alternative MI correlation length being *nearly constant* too. Our findings suggest that the characteristics of the MI length scale are markedly system-dependent and pose the question if they can capture the key features of the dynamical heterogeneity and other quasi-universal aspects of fragile glassformers.

Conflicts of interest

There are no conflicts to declare.

Acknowledgements

We acknowledge useful and fruitful comments by Carlo Andrea Massa and Francesco Puosi and the support from the project PRA-2018-34 ("ANISE") from the University of Pisa. A generous grant of computing time from IT Center, University of Pisa and Dell EMC® Italia is also gratefully acknowledged.

Notes and references

1 P. G. Debenedetti, *Metastable Liquids*, Princeton University Press, Princeton USA, 1997.
2 L. Berthier and G. Biroli, *Rev. Mod. Phys.*, 2011, **83**, 587–645.
3 G. Adam and J. H. Gibbs, *J. Chem. Phys.*, 1965, **43**, 139–146.
4 S. Karmakar, C. Dasgupta and S. Sastry, *Reports on Progress in Physics*, 2015, **79**, 016601.
5 S. Albert, T. Bauer, M. Michl, G. Biroli, J.-P. Bouchaud, A. Loidl, P. Lunkenheimer, R. Tourbot, C. Wiertel-Gasquet and F. Ladieu, *Science*, 2016, **352**, 1308–1311.
6 G. Biroli, S. Karmakar and I. Procaccia, *Phys. Rev. Lett.*, 2013, **111**, 165701.
7 M. Wyart and M. E. Cates, *Phys. Rev. Lett.*, 2017, **119**, 195501.
8 R. Richert, *J. Phys.: Condens. Matter*, 2002, **14**, R703–R738.
9 F. W. Starr, J. F. Douglas and S. Sastry, *The Journal of Chemical Physics*, 2013, **138**, 12A541.
10 T. M. Cover and J. A. Thomas, *Elements of Information Theory*, Wiley-Interscience, New York, 2006.
11 A. Kraskov, H. Stögbauer and P. Grassberger, *Phys. Rev. E*, 2004, **69**, 066138.
12 W. Li, *Journal of Statistical Physics*, 1990, **60**, 823–837.
13 J. Iaconis, S. Inglis, A. B. Kallin and R. G. Melko, *Physical Review B*, 2013, **87**, 195134.
14 P. V. Sriluckshmy and I. Mandal, *Journal of Statistical Mechanics: Theory and Experiment*, 2018, **2018**, 043301.
15 M. C. Gao and M. Widom, *The Journal of Physical Chemistry B*, 2018, **122**, 3550–3555.
16 A. J. Dunleavy, K. Wiesner and C. P. Royall, *Phys. Rev. E*, 2012, **86**, 041505.
17 R. L. Jack, A. J. Dunleavy and C. P. Royall, *Phys. Rev. Lett.*, 2014, **113**, 095703.
18 A. J. Dunleavy, K. Wiesner, R. Yamamoto and C. P. Royall, *Nature Communications*, 2015, **6**, 6089.
19 A. Widmer-Cooper, P. Harrowell and H. Fynewever, *Phys. Rev. Lett.*, 2004, **93**, 135701.
20 F. Puosi and D. Leporini, *J. Chem. Phys.*, 2012, **136**, 164901.
21 F. Puosi and D. Leporini, *J. Chem. Phys.*, 2013, **139**, 029901.
22 S. Plimpton, *J. Comput. Phys.*, 1995, **117**, 1–19.
23 *http://lammps.sandia.gov*.
24 D. Leporini, *Phys. Rev. A*, 1994, **49**, 992–1014.
25 M. Doi and S. F. Edwards, *The Theory of Polymer Dynamics*, Clarendon Press, 1988.
26 A. Barbieri, G. Gorini and D. Leporini, *Phys. Rev. E*, 2004, **69**, 061509.
27 L. Andreozzi, M. Faetti, M. Giordano and D. Leporini, *J.Phys.:Condens. Matter*, 1999, **11**, A131–A137.
28 L. Andreozzi, M. Faetti, M. Giordano and D. Leporini, *The Journal of Physical Chemistry B*, 1999, **103**, 4097–4103.
29 J. P. Hansen and I. R. McDonald, *Theory of Simple Liquids, 3rd Ed.*, Academic Press, 2006.
30 L. Larini, A. Ottochian, C. De Michele and D. Leporini, *Nature Physics*, 2008, **4**, 42–45.
31 F. Puosi and D. Leporini, *J.Phys. Chem. B*, 2011, **115**, 14046–14051.
32 A. Ottochian, C. De Michele and D. Leporini, *Philosophical Magazine*, 2008, **88**, 4057–4062.
33 F. Puosi, C. D. Michele and D. Leporini, *J. Chem. Phys.*, 2013, **138**, 12A532.
34 C. De Michele and D. Leporini, *Phys. Rev. E*, 2001, **63**, 036701.
35 R. W. Hall and P. G. Wolynes, *J. Chem. Phys.*, 1987, **86**, 2943–2948.
36 A. Ottochian, C. De Michele and D. Leporini, *J. Chem. Phys.*, 2009, **131**, 224517.
37 A. Ottochian and D. Leporini, *Philosophical Magazine*, 2011, **91**, 1786–1795.
38 A. Ottochian and D. Leporini, *J. Non-Cryst. Solids*, 2011, **357**, 298–301.
39 C. De Michele, E. Del Gado and D. Leporini, *Soft Matter*, 2011, **7**, 4025–4031.
40 F. Puosi and D. Leporini, *J. Chem. Phys.*, 2012, **136**, 211101.
41 D. S. Simmons, M. T. Cicerone, Q. Zhong, M. Tyagic and J. F. Douglas, *Soft Matter*, 2012, **8**, 11455–11461.
42 A. Ottochian, F. Puosi, C. D. Michele and D. Leporini, *Soft Matter*, 2013, **9**, 7890–7891.
43 V. N. Novikov and A. P. Sokolov, *Phys. Rev. Lett.*, 2013, **110**, 065701.
44 F. Puosi, O. Chulkin, S. Bernini, S. Capaccioli and D. Leporini, *J. Chem. Phys.*, 2016, **145**, 234904.
45 E. Guillaud, L. Joly, D. de Ligny and S. Merabia, *The Journal of Chemical Physics*, 2017, **147**, 014504.
46 R. Horstmann and M. Vogel, *The Journal of Chemical Physics*, 2017, **147**, 034505.
47 F. Puosi and D. Leporini, *J. Chem. Phys.*, 2018, **148**, 131102.
48 M. Becchi, A. Giuntoli and D. Leporini, *Soft Matter*, 2018, **14**, 8814–8820.
49 M. Kröger, *Phys. Rep.*, 2004, **390**, 453–551.
50 S. Bernini, F. Puosi, M. Barucco and D. Leporini, *J. Chem. Phys.*, 2013, **139**, 184501.
51 T. Narumi and M. Tokuyama, *Philosophical Magazine*, 2008, **88**, 4169–4175.
52 S. Bernini and D. Leporini, *The Journal of Chemical Physics*, 2016, **144**, 144505.
53 F. Puosi and D. Leporini, *J. Chem. Phys.*, 2012, **136**, 041104.
54 F. Puosi and D. Leporini, *Eur. Phys. J. E*, 2015, **38**, 87.
55 R. Higler, J. Krausser, J. van der Gucht, A. Zaccone and J. Sprakel, *Soft Matter*, 2018, **14**, 780–788.